CRYSTAL GROWTH & DESIGN

pubs.acs.org/crystal

Article

# Exploiting Strong {$Cr^{III}$–$Dy^{III}$} Ferromagnetic Exchange Coupling to Quench Quantum Tunneling of Magnetization in a Novel {$Cr^{III}_2Dy^{III}_3$} Single-Molecule Magnet

*Published as part of a Crystal Growth and Design virtual special issue on Molecular Magnets and Switchable Magnetic Materials*

Deepanshu Chauhan, Kuduva R. Vignesh,* Abinash Swain, Stuart K. Langley, Keith S. Murray, Maheswaran Shanmugam,* and Gopalan Rajaraman*

Cite This: *Cryst. Growth Des.* 2023, 23, 197–206

Read Online

ACCESS | Metrics & More | Article Recommendations | Supporting Information

**ABSTRACT:** The {3d–4f} pentanuclear complexes with the formula $[Cr^{III}_2Ln^{III}_3(PhCO_2)_7(OH)_6(^iPrO)(NO_3)(H_2O)_3]$ ($^i$PrO = isopropoxide) (where Ln = Dy (**1**), Gd (**2**)) have been synthesized and characterized using magnetic and theoretical studies. The metal core of complexes **1** and **2** has a trigonal bipyramidal arrangement with three $Ln^{III}$ ions in the triangular plane and two $Cr^{III}$ ions occupying the axial positions. These ions are held together by six $\mu_3$-OH bridges and seven carboxylate bridges. The dc magnetic susceptibility data reveal ferromagnetic interactions presiding between $Cr^{III}$ and $Ln^{III}$ ions in **1** and **2**. The fitting of the susceptibility curve employing the DFT calculated $J$ (vide infra), yield $J_{Gd^{III}-Gd^{III}}$ = +0.008 $cm^{-1}$, $J_{Cr^{III}-Gd^{III}}$ = +0.27 $cm^{-1}$, and $J_{Cr^{III}-Cr^{III}}$ = −0.007 $cm^{-1}$ for **2**. The dynamic (ac) magnetic susceptibility studies on **1** indicate slow relaxation of magnetization with a $U_{eff}$ value of 30.9 K (21.4 $cm^{-1}$) and $\tau_0 = 4.09 \times 10^{-10}$ s. These extracted parameters are among the highest for any reported {$Cr^{III}Dy^{III}$} complexes. DFT and *ab initio* CASSCF/RASSI–SO/SINGLE_ANISO/POLY_ANISO calculations were carried out to estimate the exchange interactions and their role in quenching the quantum tunneling of magnetization (QTM) behavior. *Ab initio* calculations on the $Dy^{III}$ ions reveal three asymmetric $Dy^{III}$ centers with the estimated single ion barrier in the range of 78–184 $cm^{-1}$, however, with a large QTM probability. Despite a triangular {$Dy_3$} motif, the $g_{zz}$ axes do not align in the triangular plane as observed in the {$Cr^{III}Dy^{III}_6$} single-molecule toroids (SMT) reported earlier by us. This is essentially due to the presence/absence of the $^i$PrO$^-$/carboxylate group that alters the charge distribution around the $Dy^{III}$ ion and hence the orientation of the corresponding $g_{zz}$ axis. The combination of DFT and *ab initio* CASSCF calculations yield $J_{Dy^{III}-Dy^{III}}$ = +0.012 $cm^{-1}$, $J_{Cr^{III}-Dy^{III}}$ = +1.20 $cm^{-1}$, and $J_{Cr^{III}-Cr^{III}}$ = −0.95 $cm^{-1}$ for **1**. The mechanism of magnetization relaxation developed for the {$Cr^{III}_2Dy^{III}_3$} cluster reveals that the relatively strong ferromagnetic $Cr^{III}$–$Dy^{III}$ exchange interaction reduces the ground state QTM significantly yielding a $U_{eff}$ of 38.6 $cm^{-1}$, which agrees with the experimental value. Thus, our study iterates the importance of $Cr^{III}$ ion to enhance the exchange coupling in the {3d–4f} family of clusters.

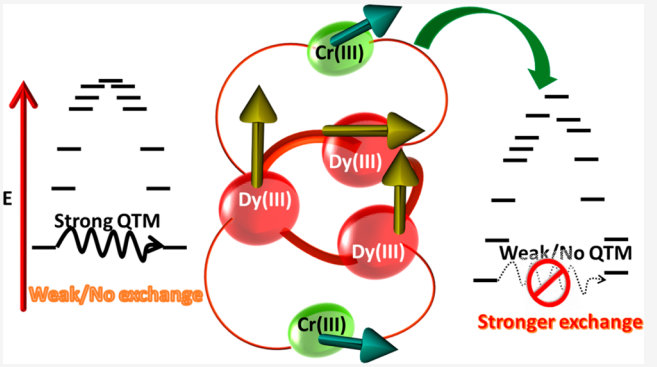


## INTRODUCTION

After the discovery of the first Single-Molecule Magnet (SMM),[1] there has been substantial growth in the field of molecule-based magnetic materials. These include the discovery of single–ion magnets (SIMs),[2] single–chain magnets (SCMs),[3] spin qubits,[4] spintronic materials,[5] and SMTs.[6] In particular, molecules that possess slow magnetization relaxation under a certain temperature are known as SMMs.[7] SMMs have magnetic bistable ground states, which can be controlled by applying an external magnetic field, revealing magnetic hysteresis. Several important breakthrough discoveries have been made in recent years using the $Dy^{III}$ ion, such as $[Dy(Cp^{ttt})_2]^+$ ($Cp^{ttt}$ = 1,2,4–tri(*tert*-butyl)-cyclopentadiene)[8] with a $U_{eff}$ and $T_B$ of 1223 $cm^{-1}$ and 60 K, respectively, by using an average sweep rate of 22 Oe $s^{-1}$, $[Dy(Cp^{iPr5})_2]^+$ ($Cp^{iPr5}$ = penta-iso-propylcyclopentadienyl)[9]

Received: August 4, 2022
Revised: November 24, 2022
Published: December 21, 2022

Table 1. Some Representative Examples of {$Cr^{III}Dy^{III}$} Complexes, Selected Structural Parameters, and Magnetic Characteristics

| Sample No. | Complexes | Cr−Dy Distance (Å) | Cr-O-Dy angle (deg) | Exchange Interactions ($Cr^{III}$–$Dy^{III}$) in $cm^{-1}$ | $U_{eff}$ (K) | $\tau_0$ (s) | ref. |
|---|---|---|---|---|---|---|---|
| 1. | $[Cr(phen)_2(\mu\text{-}MeO)_2Dy(NO_3)_4]\cdot x MeOH$ | 3.420 | 106.8 | −0.04 | - | - | 26 |
| 2. | $[DyCr(bipy)_2(\mu_2\text{-}OH)_2(H_2O)_6].(ClO_4)_4\cdot H_2O$ | 3.417 | 107.2 | −0.07 | - | - | 37 |
| 3. | $[DyCr_2(bipy)_4(\mu_2\text{-}OH)_4(H_2O)_4].(ClO_4)_5\cdot H_2O$ | 3.449 | 107.1 | −0.02 | - | - | 37 |
| 4. | $[Cr_4Dy_4(\mu_3\text{-}OH)_4(\mu\text{-}N_3)_4(mdea)_4^-(piv)_4]\cdot 3CH_2Cl_2$ | 3.333 | 98.7 | −4.50 | 15 | $1.9 \times 10^{-7}$ | 22 |
| 5. | $[Cr_8Dy_8(mdea)_{16}(CH_3COO)_8(NO_3)_8]\cdot x CH_3CN$ | 3.329−3.346 | 102.3−107.3 | −0.37/ −1.72 | 19 | $3.5 \times 10^{-8}$ | 34 |
| 6. | $[Cr_2Dy_2(OMe)_2(O_2CPh)_4(mdea)_2(NO_3)_2]$ | 3.290−3.302 | 102.7−103.3 | −16.70/ −20.30 | 77 | $5.1 \times 10^{-8}$ | 15 |
| 7. | $[Cr_2Dy_2(OMe)_2(mdea)_2(acac)_4(NO_3)_2]$ | 3.352−3.410 | 97.20−96.64 | −11.24/ −8.33 | 34.6 | $1.2 \times 10^{-7}$ | 31 |
| 8. | $[Cr_2Dy_2(OMe)_2(edea)_2(ac\ ac)_4(NO_3)_2]$ | 3.343−3.400 | 97.30−97.46 | −11.83/ −7.96 | 41.6 | $9.2 \times 10^{-8}$ | 31 |
| 9. | $[Cr_2Dy_2(OMe)_2(bdea)_2(ac\ ac)_4(NO_3)_2]$ | 3.346−3.423 | 97.72−96.12 | −10.48/ −7.14 | 37.5 | $3.1 \times 10^{-7}$ | 31 |
| 10. | $[Cr_2Dy_2(\mu_3\text{-}OH)_2(p\text{-}Me\text{-}PhCO_2)_6(L)_2]$ | 3.431−3.440 | 101.30−106.03 | −1.15 | - | - | 31 |
| 11. | $[CrDy_6(OH)_8(O\text{-}tol)_{12}(NO_3)(MeOH)_5]\cdot 3MeOH$ | 3.458 | 102.9 | −0.08 | - | - | 31 |
| 12. | $\{[Cr_2Dy_3L_{10}(OH)_6(H_2O)_2]\ Et_3NH\}$ | 3.463−3.485 | 103.2−103.7 | - | 10 | $1.3 \times 10^{-9}$ | 25 |
| 13. | $Na_3[Dy_3Cr_2(HGly)_6(\mu_3\text{-}OH)_6(H2O)_9]\cdot(ClO_4)_8\cdot Cl_4\cdot 14H_2O$ | 3.4 | 102.7−104.2 | - | 12.6 | $1.07 \times 10^{-7}$ | 35 |
| 14. | $[Cr^{III}_2Dy^{III}_3(Benz)_7(OH)_6(^iPrO)(NO_3)(H_2O)_3]$ | 3.412−3.470 | 102.8−104.02 | 1.20 | 30.9 | $4.09 \times 10^{-10}$ | this work |

exhibiting a $U_{eff}$ of 1468 $cm^{-1}$ and $T_B$ of 72 K at a sweep rate of 3.1 mT $s^{-1}$, $[(Cp^{iPr5})Dy(Cp^*)]^+$ ($Cp^{iPr5}$ = penta-isopropylcyclopentadienyl, Cp* = penta-methyl-cyclopentadienyl)[10] with a $U_{eff}$ of 1541 $cm^{-1}$ and $T_B$ value of 80 K by using a field sweep rate of 25 Oe $s^{-1}$, and a recently reported $[(Cp^{iPr5})Dy_2I_3]$[11] exhibiting a $U_{eff}$ of 1631 $cm^{-1}$ and a $T_B$ of 72 K at a sweep rate of 100 Oe $s^{-1}$. On the other hand, another class of compounds emerged over the years where the magnetic dipoles of the lanthanide ions in a vortex (circular) arrangement led to the generation of a toroidal moment perpendicular to the plane of the vortex. This class of molecules is termed single-molecule toroids or SMTs. SMTs have bistable toroidal states, and these states are nonmagnetic.[12] Notably, the magnetic field generated by toroidal moments decays more quickly than the field generated by a magnetic dipole; as a result, memory storage devices or qubits constructed using toroidal moments will be more densely packed than SMMs or spin qubits, respectively. These molecular-based magnetic materials are most promising for use in multiferroic materials, quantum computing, and information storage in the future.[7] The nature of magnetic exchange and dipolar interactions plays a pivotal role in determining the SMMs and SMTs characteristics of a particular multinuclear metal complex. The dipolar coupling plays a dominant role in SMTs, and often, this overrides the intramolecular antiferromagnetic exchange interaction between two $Ln^{III}$ ions.[12]

Generally, the exchange interaction between the $Ln^{III}$–$Ln^{III}$ centers is often very small (in the range of 0.1 to 1 $cm^{-1}$) and leads to problems in terms of magnetic relaxation, as weak exchange often leads to fast relaxation in neighboring ions via quantum tunneling of magnetization (QTM) due to transverse dipolar magnetic fields. Incorporating a radical or a 3d metal ion in the cluster aggregation solves this problem, as this often enhances the exchange by 1 or 2 orders of magnitude. Particularly, radicals were found to yield stronger exchange, and this is exemplified in several examples, including a report of two dinuclear lanthanide single-molecule magnets $[(\{Me_3Si)_2N\}_2\{THF\}Ln)_2(\mu\text{-}\eta^2\text{:}\eta^2\text{-}N_2)]^{-1}$ (Ln = Gd, Tb, or Dy), where the localized nature of the unpaired spin in the radical $N_2^{3-}$ bridge offers strong exchange with $Gd^{III}$, $Tb^{III}$, and $Dy^{III}$ ions, resulting in strong intramolecular exchange coupling. These systems were reported to have enormous thermal energy barriers of 326 and 177 K, combined with the strong magnetic exchange interaction, causing reduced QTM, greatly increasing the relaxation time. Very high blocking temperatures of $T_B$ = 14 K using a field sweep rate of 0.9 mT $s^{-1}$ and 8.3 K at a sweep rate of 0.08 T $s^{-1}$ were thus recorded for the $Tb^{III}$ and $Dy^{III}$ complexes, respectively.[13,14]

The main problem with utilizing radicals is stability, as such molecules are often unstable under ambient conditions, so device fabrication using such a class of molecules is extremely challenging. An alternative way to enhance exchange coupling is to employ 3d metals in cluster aggregation. In this regard, the $[Cr^{III}_2Dy^{III}_2(OMe)_2(O_2CPh)_4(mdea)_2(NO_3)_2]$ (mdea = *N*-methyl diethanolamine) molecule reported by some of us, exhibiting SMM behavior, gained significant attention, as the strong exchange was observed between the $Cr^{III}$–$Dy^{III}$ ions in this class of molecule leading to attractive SMM characteristics.[15] Following research on the butterfly $\{Co^{III}_2Dy^{III}_2\}$ SMM complex, which made use of the diamagnetic $Co^{III}$ ion, this $\{Cr^{III}_2Dy^{III}_2\}$ complex was chosen as a target.[16] By inserting the paramagnetic $Cr^{III}$ ($d^3$ configuration) ion into a simple tetranuclear core, the exchange interactions are enabled, which further allowed us to investigate the impact of the paramagnetic ion on magnetic relaxation. Significant $Cr^{III}$–$Dy^{III}$ antiferromagnetic exchange was in fact discovered ($J$ values between −16 and −20 $cm^{-1}$), and the relaxation times improved long enough, which were completely absent in the $\{Co^{III}_2Dy^{III}_2\}$ case.

Because of its isotropic character, the use of $Cr^{III}$ ion is frequently disregarded; yet, it can induce a strong 3d−4f interaction, yielding strong SMM characteristics compared to other 3d metals.[17,18] Importantly, 3d-$Ln^{III}$ polynuclear coordination complexes synthesized using dicationic and tricationic 3d ions such as Cr, Mn, Fe, and Co and lanthanide


https://doi.org/10.1021/acs.cgd.2c00888
Cryst. Growth Des. 2023, 23, 197−206

Table 2. Computed Magnetic Exchange Interactions ($cm^{-1}$) between Magnetic Ions in Complexes 1 and 2

| | Magnetic exchange interaction | | | | | | | | | | | |
|---|---|---|---|---|---|---|---|---|---|---|---|---|
| | DFT calculated [$cm^{-1}$] | | | *Ab initio* computed [$cm^{-1}$] | | | | | | | | |
| Complex | $J_1$ | $J_2$ | $J_3$ | $J_{1tot}$ | $J_{1ex}$ | $J_{1dip}$ | $J_{2total}$ | $J_{2ex}$ | $J_{2dip}$ | $J_{3total}$ | $J_{3ex}$ | $J_{3dip}$ |
| **1** | 0.010 | 0.99 | −0.558 | 0.012 | 0.09 | 0.03 | 1.20 | 1.16 | 0.04 | −0.95 | −0.97 | 0.02 |
| **2** | 0.015 | 1.386 | −0.558 | | | | | - | | | | |

ions have led to significant magnetic exchange interactions, therefore showing enhanced/interesting SMMs/SMTs behavior.[19] To the best of our knowledge, the design of $Cr^{III}$ and $Ln^{III}$ complexes is based on five main chemical bridging pathways. The first approach is fluoride bridging {$Cr^{III}$-F-$Ln^{III}$};[20] the second targets cyano bridged {$Cr^{III}$-CN-$Ln^{III}$} complexes;[21] the third, fourth, and fifth strategies incorporate oxo (hydroxo, methoxy etc.) {$Cr^{III}$-O-$Ln^{III}$},[22,23] oxalate {$Cr^{III}$-OOCCOO-$Ln^{III}$},[24] and carboxylate bridging {$Cr^{III}$-OCO-$Ln^{III}$} in the cluster formation.[25] In most of the $Cr^{III}$-$Dy^{III}$ complexes, the intramolecular exchange interactions between $Cr^{III}$ and $Dy^{III}$ ions were found to be antiferromagnetic (see Table 1). Examples include {$Cr^{III}Dy^{III}$},[26,27] {$Cr^{III}_2Dy^{III}$},[28] {$Cr^{III}_4Dy^{III}$},[29] {$Cr^{III}Dy^{III}_2$},[30] {$Cr^{III}Dy^{III}_6$},[31] {$Cr^{III}_2Dy^{III}_2$},[32] {$Cr^{III}_4Dy^{III}_4$},[33] and {$Cr^{III}_8Dy^{III}_8$}.[34] Notably and promisingly we see from the data that strong antiferromagnetic exchange interactions have been reported, extremely desirable for SMM design. However, examples with a ferromagnetic exchange between $Cr^{III}$ and $Dy^{III}$ are very rare, and only {$Cr^{III}_2Dy^{III}_3$}[25,23,35] and {$Cr^{III}_2Dy^{III}_4$}[36] complexes likely possess ferromagnetic exchange between $Cr^{III}$−$Dy^{III}$ ions, though these were not reported/extracted. Recently, we showed using both experimental and theoretical investigations to attain a rare ferrotoroidal phenomena utilizing antiferromagnetic and dipolar interactions in a series of heptanuclear {$Cr^{III}Ln^{III}_6$} (Ln = $Dy^{III}$, $Tb^{III}$, and $Ho^{III}$) complexes in which a $Cr^{III}$ ion links two {$Ln^{III}_3$} triangles.[31]

Here we report the heterometallic {$Cr^{III}_2Ln^{III}_3$} complexes with the molecular formula of [$Cr^{III}_2Ln^{III}_3$(Benz)$_7$(OH)$_6$($^i$PrO)(NO$_3$)(H$_2$O)$_3$] (where Ln = Dy (**1**), Gd (**2**)) possessing a triangular structural motif of $Ln^{III}$ ions with $Cr^{III}$ ions lying above and below the triangle, similar to the {$Cr^{III}Dy^{III}_6$} ferrotoroidal structure.[36,37] Complex **1** and **2** are characterized thoroughly by magnetic and theoretical studies. Unlike the reported ferrotoridal family of complexes, alteration of *ortho*-toluic acid to benzoic acid destroys the toroidal moments, but a relatively strong $Cr^{III}$−$Dy^{III}$ ferromagnetic exchange was found to yield reasonable SMM behavior.

## EXPERIMENTAL SECTION

**Synthesis of [$Cr^{III}_2Ln^{III}_3$(Benz)$_7$(OH)$_6$ ($^i$PrO)(NO$_3$)(H$_2$O)$_3$].** Cr(NO$_3$)$_3$·9H$_2$O (1 mmol, 0.400 g) and Ln(NO$_3$)$_3$·5H$_2$O (0.5 mmol, 0.22 g) were dissolved in 20 mL of acetonitrile, followed by the addition of benzoic acid (1 mmol, 0.122 g) and triethylamine base (4 mmol, 0.55 mL). This solution was stirred for 4 h at an ambient temperature. After this time, the solvent was removed, and a gel was formed. Redissolving the gel in 20 mL $^i$PrOH solution yielded suitable single crystals of purple color for X-ray analysis after a week of evaporation, with an approximate yield of 45% (crystalline product). Anal. Calcd (found) for **1** and **2**, $Cr_2Ln_3O_{27}N_1C_{52}H_{54}$: C, 36.39 (36.79); H, 3.17 (3.35); N, 0.82 (0.85) (see crystallographic data in Tables S3 and S5).

**Computational Details.** *DFT Studies.* To compute the exchange interaction, we have employed DFT calculations using the Broken Symmetry (BS) approach[38] on the crystal structure of complex **2**. The BS approach has a track record of producing accurate numerical estimates of $J$ constants earlier. Here, we have used the TZVP basis set for $Cr^{III}$ ion and the double-$\zeta$ quality basis set employing Cundari−Stevens (CS) relativistic effective core potential on Gd,[39] and Ahlrich's[40] TZV basis set for the rest atoms. The theoretical analysis section describes how this Hamiltonian was created. The exchange interaction Hamiltonian employed was as follows ($J$):

$$\hat{H} = -[J_1(S_{Ln1}S_{Ln2} + S_{Ln2}S_{Ln3} + S_{Ln3}S_{Ln1}) + J_2(S_{Cr1}S_{Ln1} + S_{Cr1}S_{Ln2} + S_{Cr1}S_{Ln3} + S_{Cr2}S_{Ln1} + S_{Cr2}S_{Ln2} + S_{Cr2}S_{Ln3}) + J_3(S_{Cr1}S_{Cr2})]$$

*Ab initio Calculations.* *Ab initio* calculations based on CASSCF/RASSI-SO/SINGLE_ANISO were performed on individual $Dy^{III}$ and $Cr^{III}$ ions on the crystal structure without any further geometry optimization using the MOLCAS 8.2 suite of programs.[41] For the computation of the magnetic properties for a single paramagnetic $Dy^{III}$ ion, the other $Dy^{III}$ ions are replaced by diamagnetic $La^{III}$ ions, and the $Cr^{III}$ ions are replaced by diamagnetic $Sc^{III}$ ions. The relativistic effects are considered based on Douglas−Kroll Hamiltonian.[42] By using the complete active space self-consistent field (CASSCF) technique, the spin-free eigenstates were attained.[43] Since we are primarily interested in the ligand field states, the 4f orbitals (CAS (9 in 7)) were included to the active space for the CASSCF calculation of the dysprosium fragment. The active space for the CASSCF calculation of the $Cr^{III}$ fragment included three electrons in five 3d orbitals. In this case, the Configuration Interaction (CI) approach was used to determine the anisotropy for the $Dy^{III}$ ion while considering the excited states of 224 quartets, 490 doublets, and 21 sextets.[44] The CASSCF module has computed each excited state associated with each multiple of ions. After computing all excited states, the spin−orbit coupled states were calculated by combining all the low-lying excited states with the RASSI-SO module.[45] Furthermore, using the SINGLE_ANISO program, the computed SO states have been considered in to compute the g-tensor to get the three main anisotropy axes and their corresponding $g_{xx}$, $g_{yy}$, and $g_{zz}$ values.[46] By using the SINGLE_ANISO code, we have computed the Crystal-field (CF) parameters (see Table S9).

With the help of the POLY ANISO routine[45] employing the Lines model,[46] the exchange interactions between anisotropic $Dy^{III}$ and $Cr^{III}$ ions in complex **1** have been calculated. For calculating the magnetic exchange interaction we used the following Hamiltonian:

$$\hat{H}_{ex} = -\sum_{i=1}^{3} J_i \cdot S_i \cdot S_{i+1}$$

Here $J_i = J_i^{dipolar} + J_i^{exchange}$, i.e., $J_i$ values indicates the total exchange interactions; this defines the magnetic interaction between the intramolecular metal centers. Dipolar magnetic coupling is the long-range interaction between magnetic moments, and it depends on the distance and the angle between the magnetic moments on magnetic centers. The well-known dipolar Hamiltonian reads:

$$H_{dip} = \frac{\mu_0}{4\pi} \sum_{p,q} \left( \frac{\mathbf{M}_p \cdot \mathbf{M}_q}{|R_{pq}|^3} - 3\frac{(\mathbf{M}_p \cdot R_{pq})(\mathbf{M}_q \cdot R_{pq})}{|R_{pq}|^3} \right)$$

where $\mathbf{M}_p$ and $\mathbf{M}_q$ are the magnetic moments of the $p$th and $q$th ions, respectively, and $R_{pq}$ is the distance between $p$ and $q$. The dipolar contribution to the exchange has been estimated and discussed in Table 2 (see below).


https://doi.org/10.1021/acs.cgd.2c00888
Cryst. Growth Des. 2023, 23, 197−206

**Scheme 1. Reaction Scheme Used to Isolate Complexes 1 and 2**

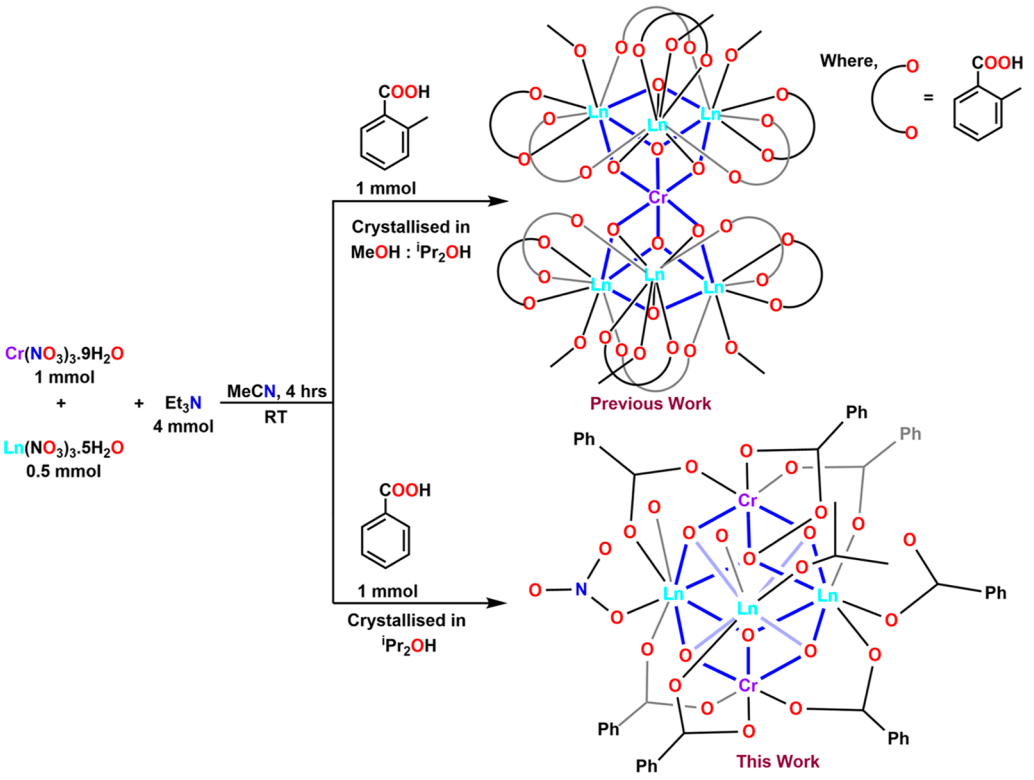


## RESULTS AND DISCUSSION

**Structural Descriptions.** The reaction of $Cr(NO_3)_3{\cdot}9H_2O$ and the respective $Ln(NO_3)_3{\cdot}5H_2O$ {Ln = Dy (**1**) and Gd (**2**)} with benzoic acid in acetonitrile at ambient temperature in the presence of triethylamine base, followed by the evaporation of the solvent and redissolution in $^{i}$PrOH, yielded a heterometallic pentanuclear complex of molecular formula $[Cr^{III}_2Ln^{III}_3(Benz)_7(OH)_6(^{i}PrO)(NO_3)(H_2O)_3]$ (where Benz = benzoate, $^{i}$PrO = isopropoxide) (Ln = Dy (**1**) Gd (**2**)) (see Scheme 1) which crystallizes in the triclinic space group $P\bar{1}$ with $Z = 1$. Complexes **1** and **2** possess trigonal bipyramidal (TBP) topology with three $Dy^{III}$ ions in the triangular plane and two $Cr^{III}$ ions, above and below the $\{Ln^{III}_3\}$ plane (see Figure 1). The central core of **1** and **2** is based on a triangle of three $Ln^{III}$ ions with $\angle Ln^{III}$-$Ln^{III}$-$Ln^{III}$ of approximately 60°, with two $Cr^{III}$ ions sitting above and below the plane of the triangle. In complex **1** the Dy−Dy distance is 3.891(3)−4.013(2) Å, the Cr−Dy distance is 3.412(2)−3.470(2) Å, and the Cr−Cr distance is 5.168 Å. The ∠Cr-O-Dy are 102.79(2)−104.02(2)°, and the ∠Cr-Dy-Cr is 96.28(3)−96.20(4)°. In complex **2** the Gd−Gd distance is 3.970(5)−4.012(4) Å, the Cr−Gd distance is 3.441−3.515 Å, and the Cr−Cr distance is 5.026(5) Å. The ∠Cr-O-Gd are 102.3(2)−104.4(2)°, and the ∠Cr-Gd-Cr is 95.63(2)−98.49(2)°. The $Cr^{III}$ ions are displaced above and below the $Ln_3$ triangles by 2.585(2) Å in **1** and 2.593(2) Å in **2** describing the $\{Cr_2^{III}Ln_3^{III}\}$ trigonal bipyramidal unit. The metal ion core is stabilized by six $\mu_3$-$OH^-$ ligands, six $\mu_2$-benzoate ligands, a single chelating nitrate and benzoate ligand, a terminal isopropoxide, and three terminal water molecules. Each $\mu_3$-$OH^-$ bridges connected through two $Ln^{III}$ ions to a $Cr^{III}$ ion, and each $\mu_2$-carboxylate bridges a $Ln^{III}$ to a $Cr^{III}$ ion. The chelating and terminal ligands complete the coordination

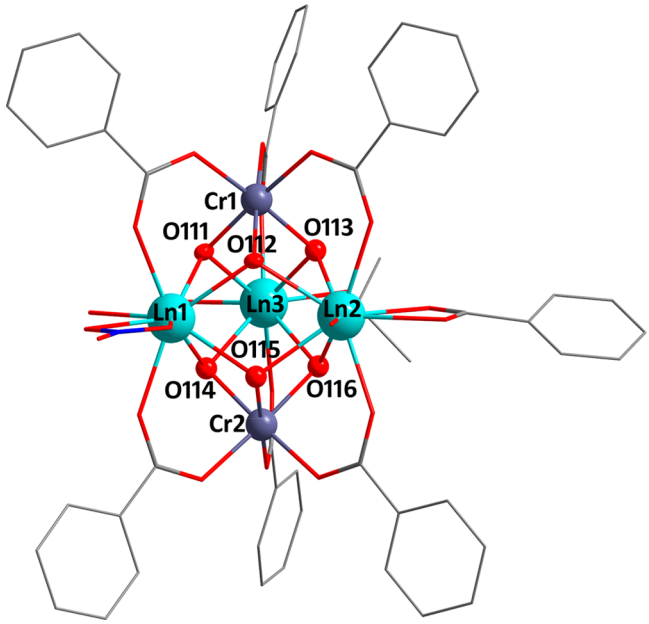


**Figure 1.** Crystal structure of **1** and **2**. Hydrogen atoms were omitted for clarity.

sphere of the $Ln^{III}$ ions. The $Cr^{III}$ ions are nearly in a perfect octahedral geometry involving six O donor sets, whereas $Ln^{III}$ ions have eight O donor coordination sites. The geometry of $Cr^{III}$ and $Ln^{III}$ centers is thoroughly examined using SHAPE 2.1 software, resulting in an octahedral geometry of Cr1 and Cr2 (with a deviation value of 0.246 and 0.215, respectively), whereas Dy1, Dy2, and Dy3 have square antiprismatic geometry ($D_{4d}$ with a deviation value 0.622, 0.712, and 0.904 from ideal square antiprismatic geometry for Dy1, Dy2, and


https://doi.org/10.1021/acs.cgd.2c00888
Cryst. Growth Des. 2023, 23, 197−206

Dy3 centers, respectively; Table S1 in SI). The packing diagram of **1** shows closely packed molecules with the shortest $Dy^{III}$–$Dy^{III}$ distance of 8.851 Å, and such close packing is associated with the intermolecular C–H $\pi$ interactions observed (see Figure 2).

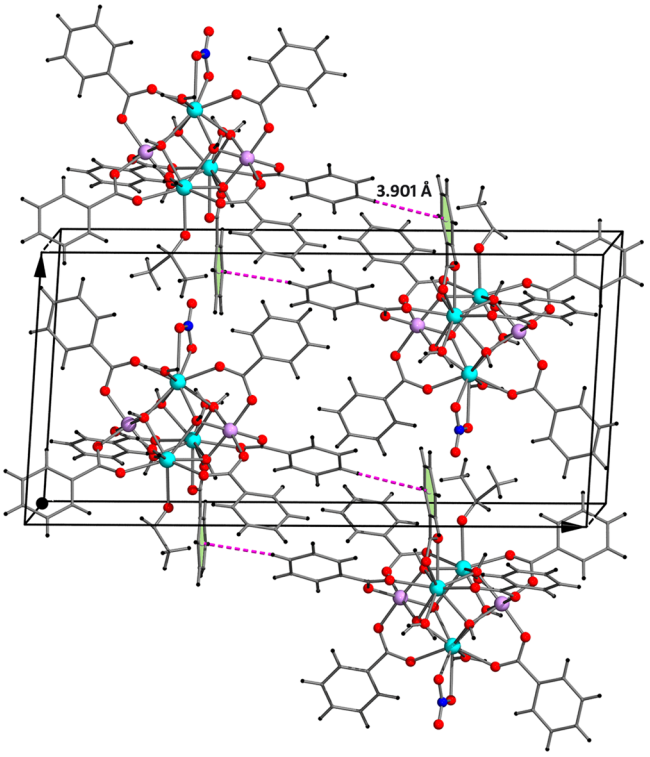


**Figure 2.** Crystal packing arrangement of complex **1** along the *a*-axis. Dashed green, cyan, violet, and orange lines indicate the C and H pi interactions between the centroids (Cg) and respective hydrogens.

**Magnetic Characterization.** The temperature-dependent dc magnetic susceptibility of a polycrystalline sample was measured from 1.8 to 300 K for both **1** and **2**. At room temperature, the $\chi_M T$ product of 45.67 $cm^3$ K $mol^{-1}$ for **1** and 27.11 $cm^3$ K $mol^{-1}$ for **2**. These values are in good agreement with the theoretical value (46.26 $cm^3$ K $mol^{-1}$ and 27.38 $cm^3$ K $mol^{-1}$ for **1** and **2**, respectively) expected for two uncoupled $Cr^{III}$ ($S$ = 3/2, $g$ = 2, $C$ = 1.875 $cm^3$ K $mol^{-1}$) and three $Dy^{III}$ ($S$ = 5/2, $L$ = 5, $^6H_{15/2}$, $g$ = 4/3, $C$ = 14.17 $cm^3$ K $mol^{-1}$) ions or three $Gd^{III}$ ($S$ = 7/2), respectively. For complex **1**, on lowering the temperature, the $\chi_M T$ products remain nearly constant down to 100.2 K, followed by a decrease down to 20.6 $cm^3$ K $mol^{-1}$ at 40.5 K. After that, a sharp increase to reach a maximum value of 101.5 $cm^3$ K $mol^{-1}$ at 1.8 K was observed for **1**. Similarly, the $\chi_M T$ products remain nearly constant up to 102.0 K. Thereafter, a sharp increase to reach a maximum value of 59.3 $cm^3$ K $mol^{-1}$ at 4.4 K was observed for **2** (see Figure 3a,b).

In the magnetic field range of 0–7 T at 2, 3, 5, and 10 K field dependence of the magnetization was studied for both **1** and **2**. For fields up to 2 T, there is an initial rapid increase at low temperatures, reaching 16.28 $\mu_B$ for **1** and 27.27 $\mu_B$ for **2**. This was followed by a slower quasi-linear increase up to 7 T, reaching 18.9 and 28.02 $\mu_B$ for **1** and **2**, respectively (see Figure 3c, d). The population of low-lying excited states and/or magnetic anisotropy could be the reason for the non-

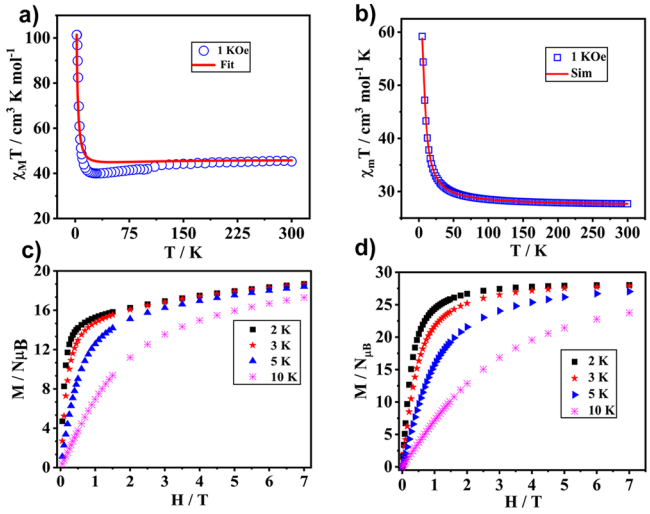


**Figure 3.** (a, b) Plot of temperature-dependent dc magnetic susceptibility ($\chi_M T$) vs temperature ($T$) for **1** and **2**, respectively. The measured (blue circle for **1** and blue square for **2**), fitted and simulated (via the *ab initio* parametrized red solid line **1** with 96.2% match and PHI simulation for **2** are in solid red line with a match of 99.9%) and (c, d) the field-dependent magnetization isotherms for **1** and **2**, respectively.

superposed reduced magnetization curves at different temperatures.

The magnetic susceptibility of complex **2** was fitted using the PHI suite with three different exchange interactions employing DFT calculations as the starting point (see below). This yield an excellent fit with the estimated $J$ values of $J_{Gd^{III}-Gd^{III}}$ = +0.008 $cm^{-1}$, $J_{Cr^{III}-Gd^{III}}$ = +0.27 $cm^{-1}$, and $J_{Cr^{III}-Cr^{III}}$ = −0.007 $cm^{-1}$ for **2**. The magnetization plot (see Figure 3d) suggests a saturation of magnetization ~27 at 2 K, suggesting a ground state of $S$ = 27/2, which is consistent with the dominant ferromagnetic coupling in the cluster.

The alternate current (ac) magnetic susceptibility measurements were performed to examine the dynamic of magnetization relaxation, which show significant in-phase ($\chi'$) and out-of-phase ($\chi''$) peaks in the 2–2.8 K temperature range for an oscillating field range of 1 to 900 Hz that are temperature- and frequency-dependent under zero dc field (see Figure 4a and b), which indicate the presence of slow relaxation of magnetization and SMM behavior. The Cole–Cole plots of $\chi'$ versus $\chi''$ from 2 to 2.8 K obtained by fitting the measurement data using a generalized Debye model (see eq 1) with $\alpha$ values ranging from 0.02 to 0.25 (see Table S2) displayed nonsymmetrical semicircles, suggest a single step relaxation process of magnetization.

$$\chi_{ac}(\omega) = \chi_S + \frac{\chi_T - \chi_S}{1 + (i\omega\tau)^{1-\alpha}} \quad (1)$$

where $\chi_S$, $\chi_T$, $\omega$, and $\tau$ represent adiabatic susceptibility, isothermal susceptibility, angular frequency, and relaxation time.

By fitting the Cole–Cole plot (see Figure 4c), relaxation times ($\tau$) were extracted to determine the effective energy barrier ($U_{eff}$). The following general equation was used to model the magnetic relaxation data considering several relaxation processes:

$$1/\tau = CT^n + \tau_0^{-1} \exp(U_{eff}/k_B T)$$


https://doi.org/10.1021/acs.cgd.2c00888
Cryst. Growth Des. 2023, 23, 197–206

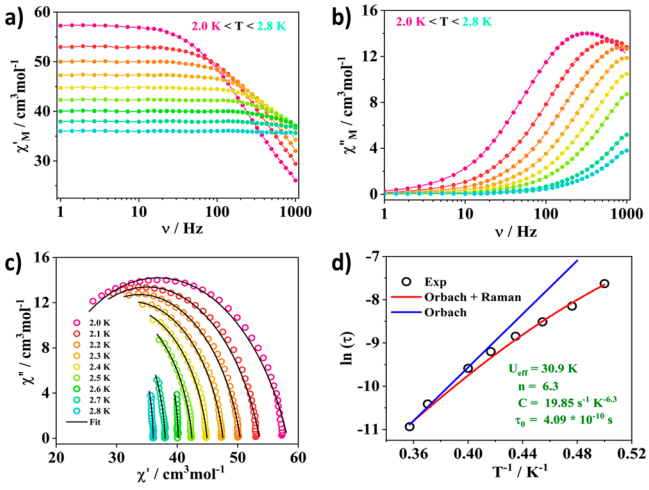


**Figure 4.** Temperature-dependence ac magnetic susceptibility measurement. (a) in-phase $\chi_M'$ and (b) out-of-phase ac magnetic susceptibilities at the shown frequencies for complex **1**. (c) Cole–Cole plot and (d) Arrhenius plot.

The Raman relaxation process is represented by the first term, and the Orbach relaxation process is represented by the second term. Many fits were tried using a number of variable parameters in the equation. The linear fit (shown by a solid blue line) relates to the Orbach relaxation pathway only. By taking into account the Orbach and Raman relaxation processes, the best fit for the Arrhenius plot was obtained, with the Raman exponent $n$ closer to 6.3. The values obtained from the best fit are $n$ = 6.3, $C$ = 19.85 $s^{-1}$ $K^{-6.3}$, $U_{eff}$ = 30.9 K (21.4 $cm^{-1}$), and $\tau_0 = 4.09 \times 10^{-10}$ s (see Figure 4d).

*Estimation of Exchange Coupling.* DFT calculations were performed on the crystal structure of complex **2** to obtain the exchange coupling between $Gd^{III}$–$Gd^{III}$ ($J_1$), $Cr^{III}$–$Gd^{III}$ ($J_2$), and $Cr^{III}$–$Cr^{III}$ ($J_3$) interactions (see Figure 7b). From these calculations, we have obtained $J_1$ = +0.015 $cm^{-1}$, $J_2$ = +1.38 $cm^{-1}$, and $J_3$ = −0.558 $cm^{-1}$ indicating a ferromagnetic interaction between $Gd^{III}$–$Gd^{III}$ and $Cr^{III}$–$Dy^{III}$, and an antiferromagnetic interaction between $Cr^{III}$–$Cr^{III}$ (see Table 2). These values are consistent with the results of the PHI fitting, though the magnitude of the $J$'s is overestimated in the DFT calculations. Both in DFT and the PHI fitting, the $Cr^{III}$–$Dy^{III}$ $J_2$ interaction is the strongest and thus dictates the magnetic properties of the cluster.

For complex **1**, the estimated exchange coupling constants corresponding to $Cr^{III}$–$Gd^{III}$ interactions were rescaled by $S$ = 5/2 (Dy(III)) as established earlier.[15,47] In the {$Cr^{III}Dy_6^{III}$} ferrotoroidal complex reported earlier, the exchange interaction between the $Cr^{III}$–$Dy^{III}$ and $Dy^{III}$–$Dy^{III}$ ions are antiferromagnetic, and this is due to the absence of a carboxylate bridge between $Cr^{III}$ and $Dy^{III}$ ions.[30] In that case, the ions are only connected via $\mu_3$-$OH^-$ bridges. In **1**, $Cr^{III}$ and $Dy^{III}$ ions are connected both via $\mu_3$-OH as well as the carboxylate bridge, and the $Cr^{III}$ magnetic orbitals were found to mix strongly with the carboxylate bridges, and such mixing offers a counter-complementarity effect and alters the sign of exchange as shown by some of us earlier in $Cr^{III}$ dimers (see also Figure S4 in SI).[48]

Further, the overlap integral between the SOMOs of $Cr^{III}$ and $Gd^{III}$ ions reveals a very weak overlap, and this diminishes the contributions from the antiferromagnetic part of the exchange (see Table S10). The strongest overlap was visible between $f_{xyz}$($Gd^{III}$) and $d_{xz}$($Cr^{III}$) orbitals (see Figure 5b), and the strength of the overlap for this pair is dictated by the $Cr^{III}$-O-$Gd^{III}$ angles. In comparison, a previously reported dinuclear $Cr^{III}$–$Gd^{III}$ dimer with an F-bridge exhibited stronger overlap leading to a net antiferromagnetic coupling.[20] Further, the computed spin density plot (see Figure 5a) reveals a strong spin polarization mechanism for both the $Cr^{III}$ and $Gd^{III}$ ions, with atoms coordinated to these ions exhibiting a large negative spin density (as much as −0.1 on the $\mu_3$-$OH^-$ bridges). Such a spin polarization mechanism also favors ferromagnetic coupling as the exchange here is mediated via an odd number of bridging atoms as per the McConnell mechanism.[49] Further, the $Cr^{III}$-O-$Gd^{III}$ angle found here is in the range of 103–104°, and this range is expected to yield ferromagnetic coupling as per the magneto-structural correlation developed earlier for various {3d-Gd} pairs.[17,18]

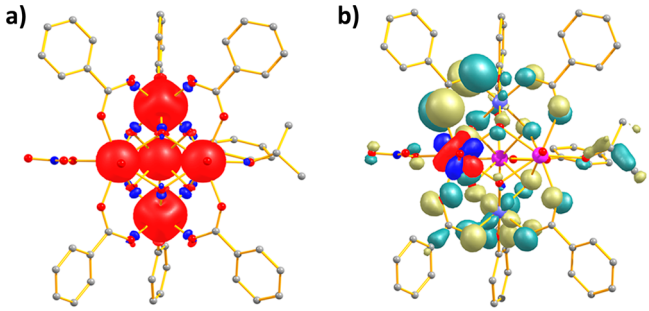


**Figure 5.** (a) DFT computed spin density plot high spin with the red and blue area representing positive and negative spin densities, respectively. (b) The representative d and f orbitals show there is no overlap. The isodensity surface shown corresponds to a value of 0.023 $e^-/bohr^3$.

Although $J_1$ and $J_3$ are small, the structural parameters observed for $J_1$, i.e., $Gd^{III}$-O-$Gd^{III}$ angles in the range of 108–110° are expected to yield an exchange value close to zero as per the magneto-structural correlation developed.[50] The values we reported fit very well within this hypothesis. Additionally, the $J_3$ interaction is strongly correlated to the $Cr^{III}$-$Gd^{III}$-$Cr^{III}$ angle as the angle here is greater than 71.50°; an antiferromagnetic $J_3$ interaction is expected based on earlier correlations.[51] While there is no direct bridging available between two $Cr^{III}$ ions, it is very well-known that the (1,3) interaction between two transition metal ions/radicals is stronger and sometimes comparable to or even exceeds the strength of (1,2) 3d–4f interactions.[17,52] This is essentially due to the fact that $Cr^{III}$ SOMOs overlap effectively via the formally empty 5d/6s orbitals of the $Ln^{III}$ ions.

*Dynamics of Magnetization from Single-Ion Anisotropy of $Dy^{III}$ Ions.* To enlighten the experimental observations, we performed *ab initio* calculations on the X-ray structure. The computed direction of the local magnetic anisotropic axes is shown in Figure 7a. The calculations yielded the following low-lying energies (see Table 3) and g-tensor principal values: (Dy1; $g_x$ = 0.0728, $g_y$ = 0.1509, and $g_z$ = 19.5221); (Dy2; $g_x$ = 0.4592, $g_y$ = 0.9379, $g_z$ = 18.6176); (Dy3; $g_x$ = 0.0036, $g_y$ = 0.0052, and $g_z$ = 19.6985); and (Cr1; $g_x = g_y = g_z$ = 1.96 and Cr2; $g_x = g_y = g_z$ = 1.96) (see Table 3). This indicates that for the Dy1 and Dy2 centers, a small but non-negligible transverse anisotropy is present in the ground state, whereas for the Dy3, a near axial anisotropy has been observed. The direction of the $g_{zz}$ axis of the Dy1 and Dy2 ions is found to be perpendicular


https://doi.org/10.1021/acs.cgd.2c00888
Cryst. Growth Des. 2023, 23, 197–206

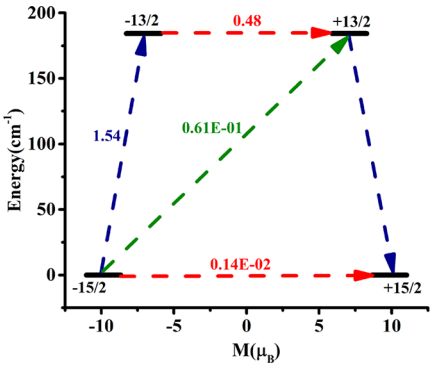


**Figure 6.** *Ab initio* computed qualitative magnetic relaxation mechanism for Dy3 ion center in **1**. The thick black line represents the KDs as a function of the magnetic moment computed. The green/blue arrows indicate a potential pathway via the Orbach/Raman relaxation. The presence of QTM and thermally assisted QTM (TA-QTM) between the connected pairs is represented by the dotted red lines. The numbers next to each arrow represent the mean absolute values of the relevant matrix element of the transition magnetic moment.

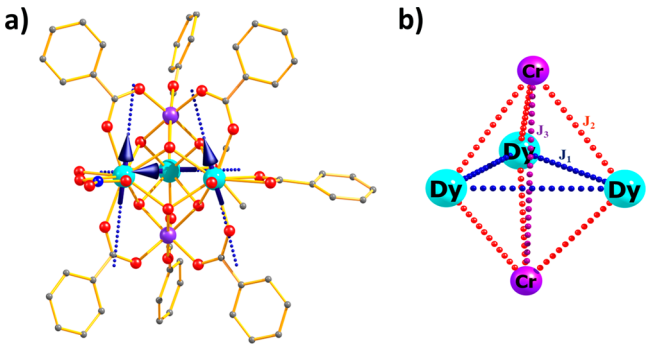


**Figure 7.** (a) The orientation of the magnetic anisotropy axes. (b) Magnetic exchange pathways $J_1$, $J_2$, and $J_3$ are highlighted.

**Table 3. Energies of the Lowest Kramers Doublets and Ground State g-Tensors of Each $Dy^{III}$ Center**

| | $E$ ($cm^{-1}$) | | |
|---|---|---|---|
| KD's | Dy1 | Dy2 | Dy3 |
| **1** | 0 | 0 | 0 |
| **2** | 78.8 | 37.3 | 184.2 |
| **3** | 154.0 | 60.9 | 236.5 |
| **4** | 192.3 | 82.2 | 291.8 |
| **5** | 207.5 | 104.5 | 367.8 |
| **6** | 239.9 | 136.8 | 442.0 |
| **7** | 276.1 | 159.3 | 451.9 |
| **8** | 434.0 | 327.0 | 734.8 |
| | g-tensor | | |
| $g_x$ | 0.0728 | 0.4592 | 0.0036 |
| $g_y$ | 0.1509 | 0.9379 | 0.0052 |
| $g_z$ | 19.5221 | 18.6176 | 19.6985 |

to the $\{Dy_3\}$ triangular motif, while for Dy3 the axis is found to be along the plane of the triangle. This arrangement does not support SMT behavior. Despite the structural resemblance to $\{CrDy_6\}$, this molecule does not exhibit SMT behavior as the direction of the $g_{zz}$ anisotropy axes is altered.

We carefully analyze the reason behind the change, and this is essentially due to the fact that the carboxylate bridges in $\{Cr^{III}Dy^{III}{}_6\}$ lie in the plane of the $\{Dy_3\}$ triangle, and this geometry is enforced due to the coordination of MeOH perpendicular to the plane for all three $Dy^{III}$ ions. In complex **1**, such a geometry is retained only for Dy3, where the presence of $^{i}PrO^{-}$ and the absence of a carboxylate bridge enforces the $g_{zz}$ axis to lie in the $\{Dy_3\}$ plane. The absence of $^{i}PrO^{-}$ groups and the presence of a carboxylate bridge perpendicular to the $\{Dy_3\}$ triangle in Dy1 and Dy2 alters the $g_{zz}$ direction (see Figure 8 for the LoProp charges computed). As the carboxylate oxygen of Dy1 and Dy2 has the highest negative charge, the $g_{zz}$ is found to lie along this direction. In Dy3, as the carboxylate bridge is absent, the next largest negative charge was detected at the oxygen atom of the $^{i}PrO^{-}$ group leading to the $g_{zz}$ lying along this group.

The relaxation mechanism based on a single $Dy^{III}$ ion is given in Figure 6 for Dy3 (see Figure S2 for Dy1 and Dy2). The computed energies of the eight low-lying Kramers Doublets (KDs) of individual $Dy^{III}$ ions in the complex are shown in Table 3. The energy gap between the ground and the first excited state KDs is 78.8, 37.3, and 184.2 $cm^{-1}$ for Dy1, Dy2, and Dy3, respectively. This large difference in the estimated gap is due to the difference in the charge distribution observed. The presence of the $^{i}PrO^{-}$ group in Dy3 offers the strongest axiality and leads to the largest ground state−excited state gap. The ground to first excited state energy gap is quite large compared to the experimentally obtained $U_{eff}$ value. This indicates the overall magnetic relaxation depends on the exchanged coupled states rather than the single $Dy^{III}$ ions.

The CF characteristics of complex **1** were examined in order to acquire a better understanding of the mechanism of magnetic relaxation. The equation contains the associated crystal field Hamiltonian:

$$\hat{H}_{CF} = \sum \sum_{k=-q}^{q} B_k^q \tilde{O}_k^q$$

where $B_k^q$ is the crystal field parameter and $\tilde{O}_k^q$ is the Steven's operator.

The CF parameters for **1** are given in Table S9 in the SI. In **1**, the nonaxial terms are found to be larger than axial terms, and this leads to a significant transverse anisotropy at the ground state and hence significant QTM probability. Due to such strong QTM behavior, at the single-ion level, **1** does not expect to exhibit zero-field SMM behavior.[53]

**Dynamics of Magnetization from the Exchange Coupled $\{Cr^{III}{}_2Dy^{III}{}_3\}$ System.** We used the Lines approach to fit the susceptibility with the starting values of $J_1$−$J_3$ estimated from DFT employed. A satisfactory fit to the susceptibility data yields $J_2$ = +1.20 $cm^{-1}$, which is only marginally larger than the DFT estimated value assuming isotropic $Gd^{III}$ ion (see Table 2). The magnetization relaxation mechanism developed for the coupled $\{Cr^{III}{}_2Dy^{III}{}_3\}$ is shown in Figure 9. In this case, magnetization is projected to blockade via the 17th excited doublet, resulting in a $U_{eff}$ value of 38.59 $cm^{-1}$, which is reasonably close to the experimental value (21.47 $cm^{-1}$). The ground state QTM here is estimated to be $0.91 \times 10^{-4}$ $\mu_B$, while for the single ion anisotropy, the largest ground state QTM was computed to be 0.23 $\mu_B$ for the Dy2, unveiling the extent of quenching at the ground state. The relatively strong $\{Cr^{III}$−$Dy^{III}\}$ exchange was found to quench the tunneling at the ground state and the excited states leading to a sustained SMM behavior as observed in the experiments.


https://doi.org/10.1021/acs.cgd.2c00888
Cryst. Growth Des. 2023, 23, 197−206

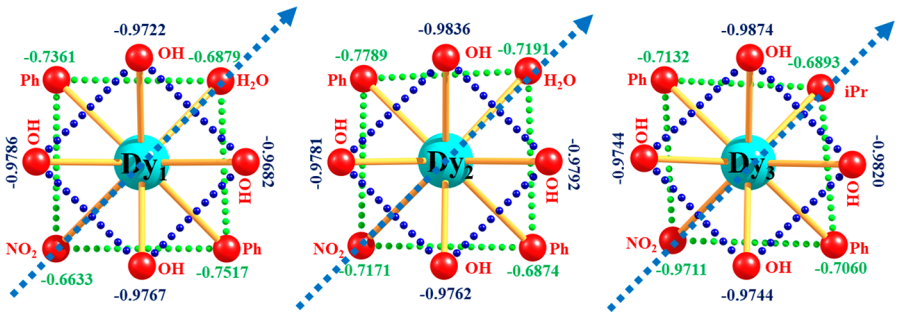


**Figure 8.** Computed LoProp charges with the label of the particular oxygen atom and magnetic anisotropic axes direction (blue arrow) of the ground state ($KD_1$) along each $Dy^{III}$ centers (left is for $Dy_1$, middle for $Dy_2$, and the right is for $Dy_3$ ions).

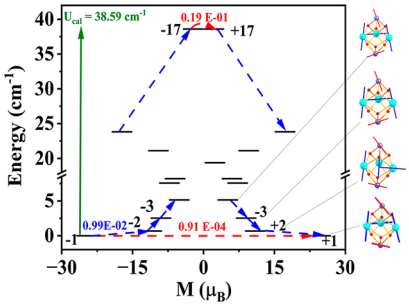


**Figure 9.** Low-lying exchange spectrum computed for the $\{Cr^{III}_2Dy^{III}_3\}$ motif. The magnetic moments of the exchange-coupled states (KDs) are represented on the diagram (bold black lines). The blue arrows indicate a possible pathway through Orbach/Raman relaxation. The existence of QTM/TA-QTM between the connecting KDs is represented by the dashed red arrows, and the effective energy barrier is represented by the green arrows.

## CONCLUSIONS

In summary, a rare $Cr^{III}$–$Dy/Gd^{III}$ SMM with the formula $[Cr^{III}_2Ln^{III}_3(Benz)_7(OH)_6(^iPrO)(NO_3)(H_2O)_3]$ (**1** = **$Dy^{III}$**, **2** = **$Gd^{III}$**) has been synthesized and characterized using magnetic and theoretical studies. Complex **1** exhibited slow magnetization relaxation with a $U_{eff}$ value of 30.9 K, while **2** exhibited a very high spin ground state of $S = 27/2$. The DFT and *ab initio* calculations highlight the importance of the structural difference between **1**/**2** and our previously reported $\{Cr^{III}Dy^{III}_6\}$ SMT. Particularly the alcohol composition combined with the alteration in the number of carboxylate bridges alter the direction of the $g_{zz}$ axis of the $Dy^{III}$ ion, thus destroying the SMT characteristics despite possessing a similar $\{Dy_3\}$ motif. Furthermore, *ab initio* and DFT calculations establish that a relatively strong ferromagnetic $Cr^{III}$–$Dy^{III}$ interaction quenches the QTM at the ground state leading to the zero-field SMM behavior for **1**. As the $Cr^{III}$–$Dy^{III}$ exchange coupling is strong (~1 $cm^{-1}$), this quenches the QTM probability of the low-lying doublets. Thus, our study highlights the importance of $Cr^{III}$ in d–f cluster aggregation to enhance the exchange coupling and simultaneously disclose the subtle SMT behavior in such a class of molecules.

## ASSOCIATED CONTENT

### Supporting Information

The Supporting Information is available free of charge at https://pubs.acs.org/doi/10.1021/acs.cgd.2c00888.

Supporting single crystal XRD data, structural parameters, shape analysis, magnetic data, and computational details (PDF)

### Accession Codes

CCDC 2191707 and 2217366 contain the supplementary crystallographic data for this paper. These data can be obtained free of charge via www.ccdc.cam.ac.uk/data_request/cif, or by emailing data_request@ccdc.cam.ac.uk, or by contacting The Cambridge Crystallographic Data Centre, 12 Union Road, Cambridge CB2 1EZ, UK; fax: +44 1223 336033.

## AUTHOR INFORMATION


### Corresponding Authors

**Gopalan Rajaraman** – *Department of Chemistry, Indian Institute of Technology Bombay, Mumbai 400076 Maharashtra, India;* orcid.org/0000-0001-6133-3026; Email: rajaraman@chem.iitb.ac.in

**Kuduva R. Vignesh** – *Department of Chemical Sciences, Indian Institute of Science Education and Research Mohali, Punjab 140306, India;* orcid.org/0000-0002-0971-2990; Email: vigneshkuduvar@iisermohali.ac.in

**Maheswaran Shanmugam** – *Department of Chemistry, Indian Institute of Technology Bombay, Mumbai 400076 Maharashtra, India*; Email: eswar@chem.iitb.ac.in

### Authors

**Deepanshu Chauhan** – *Department of Chemistry, Indian Institute of Technology Bombay, Mumbai 400076 Maharashtra, India*

**Abinash Swain** – *Department of Chemistry, Indian Institute of Technology Bombay, Mumbai 400076 Maharashtra, India*

**Stuart K. Langley** – *School of Science and the Environment, Division of Chemistry, Manchester Metropolitan University, Manchester M15 6BH, United Kingdom;* orcid.org/0000-0002-2241-1551

**Keith S. Murray** – *School of Chemistry, Monash University, Clayton, Victoria 3800, Australia*

Complete contact information is available at: https://pubs.acs.org/10.1021/acs.cgd.2c00888


### Notes

The authors declare no competing financial interest.

## ACKNOWLEDGMENTS

We thank DST and SERB (SB/SJF/2019-20/12). MS wishes to thank funding agencies SERB (CRG/2019/004185 and SPR/2019/001145), CSIR (01(2933)/18/EMR-II). DC thanks to UGC for a fellowship and IIT Bombay for central facility. KSM acknowledges receipt of an ARC Discovery grant.

## REFERENCES


(1) Sessoli, R.; Gatteschi, D.; Caneschi, A.; Novak, M. Magnetic bistability in a metal-ion cluster. *Nature* **1993**, *365* (6442), 141−143.
(2) Ishikawa, N.; Sugita, M.; Ishikawa, T.; Koshihara, S.-y.; Kaizu, Y. Lanthanide double-decker complexes functioning as magnets at the single-molecular level. *J. Am. Chem. Soc.* **2003**, *125* (29), 8694−8695.
(3) Caneschi, A.; Gatteschi, D.; Lalioti, N.; Sangregorio, C.; Sessoli, R.; Venturi, G.; Vindigni, A.; Rettori, A.; Pini, M. G.; Novak, M. A. Cobalt (II)-nitronyl nitroxide chains as molecular magnetic nanowires. *Angew. Chem., Int. Ed.* **2001**, *40* (9), 1760−1763.
(4) Fernandez, A.; Ferrando-Soria, J.; Pineda, E. M.; Tuna, F.; Vitorica-Yrezabal, I. J.; Knappke, C.; Ujma, J.; Muryn, C. A.; Timco, G. A.; Barran, P. E. Making hybrid [n]-rotaxanes as supramolecular arrays of molecular electron spin qubits. *Nat. Commun.* **2016**, *7* (1), 1−6.
(5) Bogani, L.; Wernsdorfer, W.Molecular spintronics using single-molecule magnets. In *Nanoscience and technology: a collection of reviews from nature journals*; World Scientific, 2010; pp 194−201.
(6) Chibotaru, L. F.; Ungur, L.; Soncini, A. The origin of nonmagnetic Kramers doublets in the ground state of dysprosium triangles: evidence for a toroidal magnetic moment. *Angew. Chem.* **2008**, *120* (22), 4194−4197.
(7) Zabala-Lekuona, A.; Seco, J. M.; Colacio, E. Single-Molecule Magnets: From Mn12-ac to dysprosium metallocenes, a travel in time. *Coord. Chem. Rev.* **2021**, *441*, 213984.
(8) Goodwin, C. A.; Ortu, F.; Reta, D.; Chilton, N. F.; Mills, D. P. Molecular magnetic hysteresis at 60 K in dysprosocenium. *Nature* **2017**, *548* (7668), 439−442.
(9) McClain, K. R.; Gould, C. A.; Chakarawet, K.; Teat, S. J.; Groshens, T. J.; Long, J. R.; Harvey, B. G. High-temperature magnetic blocking and magneto-structural correlations in a series of dysprosium (III) metallocenium single-molecule magnets. *Chem. Sci.* **2018**, *9* (45), 8492−8503.
(10) Guo, F.-S.; Day, B. M.; Chen, Y.-C.; Tong, M.-L.; Mansikkamäki, A.; Layfield, R. A. Magnetic hysteresis up to 80 K in a dysprosium metallocene single-molecule magnet. *Science* **2018**, *362* (6421), 1400−1403.
(11) Gould, C. A.; McClain, K. R.; Reta, D.; Kragskow, J. G.; Marchiori, D. A.; Lachman, E.; Choi, E.-S.; Analytis, J. G.; Britt, R. D.; Chilton, N. F. Ultrahard magnetism from mixed-valence dilanthanide complexes with metal-metal bonding. *Science* **2022**, *375* (6577), 198−202.
(12) Vignesh, K. R.; Rajaraman, G. Strategies to Design Single-Molecule Toroics Using Triangular {Ln3} n Motifs. *ACS omega* **2021**, *6* (48), 32349−32364.
(13) Rinehart, J. D.; Fang, M.; Evans, W. J.; Long, J. R. A $N_2^{3-}$-radical-bridged terbium complex exhibiting magnetic hysteresis at 14 K. *J. Am. Chem. Soc.* **2011**, *133* (36), 14236−14239.
(14) Rinehart, J. D.; Fang, M.; Evans, W. J.; Long, J. R. Strong exchange and magnetic blocking in $N_2^{3-}$-radical-bridged lanthanide complexes. *Nat. Chem.* **2011**, *3* (7), 538−542.
(15) Langley, S. K.; Wielechowski, D. P.; Vieru, V.; Chilton, N. F.; Moubaraki, B.; Abrahams, B. F.; Chibotaru, L. F.; Murray, K. S. A $\{Cr^{III}_2Dy^{III}_2\}$ Single-Molecule Magnet: Enhancing the Blocking Temperature through 3d Magnetic Exchange. *Angew. Chem., Int. Ed.* **2013**, *52* (46), 12014−12019.
(16) Langley, S. K.; Chilton, N. F.; Ungur, L.; Moubaraki, B.; Chibotaru, L. F.; Murray, K. S. Heterometallic tetranuclear [LnIII2CoIII2] complexes including suppression of quantum tunneling of magnetization in the $[Dy^{III}_2Co^{III}_2]$ single molecule magnet. *Inorg. Chem.* **2012**, *51* (21), 11873−11881.
(17) Singh, S. K.; Tibrewal, N. K.; Rajaraman, G. Density functional studies on dinuclear {Ni II Gd III} and trinuclear {Ni II Gd III Ni II} complexes: magnetic exchange and magneto-structural maps. *Dalton Trans.* **2011**, *40* (41), 10897−10906.
(18) Singh, S. K.; Rajaraman, G. Decisive interactions that determine ferro/antiferromagnetic coupling in {3d-4f} pairs: a case study on dinuclear {V (IV)-Gd (III)} complexes. *Dalton Trans.* **2013**, *42* (10), 3623−3630.
(19) Ashtree, J. M.; Borilović, I.; Vignesh, K. R.; Swain, A.; Hamilton, S. H.; Whyatt, Y. L.; Benjamin, S. L.; Phonsri, W.; Forsyth, C. M.; Wernsdorfer, W.; Soncini, A.; Rajaraman, G.; Langley, S. K.; Murray, K. S. Tuning the Ferrotoroidic Coupling and Magnetic Hysteresis in Double-Triangle Complexes {Dy3MIIIDy3} via the MIII-linker. *Eur. J. Inorg. Chem.* **2021**, *2021* (5), 435−444.
(20) Pedersen, K. S.; Lorusso, G.; Morales, J. J.; Weyhermüller, T.; Piligkos, S.; Singh, S. K.; Larsen, D.; Schau-Magnussen, M.; Rajaraman, G.; Evangelisti, M. Fluoride-Bridged $\{Gd^{III}_3M^{III}_2\}$(M= Cr, Fe, Ga) Molecular Magnetic Refrigerants. *Angew. Chem., Int. Ed.* **2014**, *53* (9), 2394−2397.
(21) Kou, H. Z.; Zhou, B. C.; Gao, S.; Wang, R. J. A 2D Cyano-and Oxamidato-Bridged Heterotrimetallic $Cr^{III}$-$Cu^{II}$-$Gd^{III}$ Complex. *Angew. Chem., Int. Ed.* **2003**, *42* (28), 3288−3291.
(22) Rinck, J.; Novitchi, G.; Van den Heuvel, W.; Ungur, L.; Lan, Y.; Wernsdorfer, W.; Anson, C. E.; Chibotaru, L. F.; Powell, A. K. An Octanuclear $[Cr^{III}_4Dy^{III}_4]$ 3d-4f Single-Molecule Magnet. *Angew. Chem., Int. Ed.* **2010**, *49* (41), 7583−7587.
(23) Zhao, X.-Q.; Wang, J.; Zhang, F.-H.; Sun, M.-M.; Li, Y.-C.; Wang, M.-M.; Tang, Y.-F. Significant magnetocaloric effect in a ferromagnetic $\{Cr^{III}_2Gd^{III}_3\}$ cluster. *Polyhedron* **2020**, *179*, 114385.
(24) Aboshyan-Sorgho, L.; Nozary, H.; Aebischer, A.; Bünzli, J.-C. G.; Morgantini, P.-Y.; Kittilstved, K. R.; Hauser, A.; Eliseeva, S. V.; Petoud, S. p.; Piguet, C. Optimizing millisecond time scale near-infrared emission in polynuclear chrome (III)-lanthanide (III) complexes. *J. Am. Chem. Soc.* **2012**, *134* (30), 12675−12684.
(25) Wang, X. Q.; Li, Z. Y.; Zhu, Z. X.; Zhu, J.; Liu, S. Q.; Ni, J.; Zhang, J. J. Pentanuclear $\{Cr_2Ln_3\}$(Ln= Dy, Tb) Heterometallic Clusters Based on an Amino Acid Ligand: Slow Relaxation of Magnetization and Substitution Reactions. *Eur. J. Inorg. Chem.* **2013**, *2013* (29), 5153−5160.
(26) Dreiser, J.; Pedersen, K. S.; Birk, T.; Schau-Magnussen, M.; Piamonteze, C.; Rusponi, S.; Weyhermüller, T.; Brune, H.; Nolting, F.; Bendix, J. X-ray magnetic circular dichroism (XMCD) study of a methoxide-bridged DyIII-CrIII cluster obtained by fluoride abstraction from cis-$[Cr^{III}F_2(phen)_2]^+$. *J. Phys. Chem. A* **2012**, *116* (30), 7842−7847.
(27) Dreiser, J.; Pedersen, K. S.; Piamonteze, C.; Rusponi, S.; Salman, Z.; Ali, M. E.; Schau-Magnussen, M.; Thuesen, C. A.; Piligkos, S.; Weihe, H. Direct observation of a ferri-to-ferromagnetic transition in a fluoride-bridged 3d-4f molecular cluster. *Chem. Sci.* **2012**, *3* (4), 1024−1032.
(28) Li, Z.-Y.; Wang, X.-Q.; Zhang, J.-J.; Liu, S.-Q.; Ni, J.; Sun, Y.-J. Synthesis, Structures, and Magnetic Properties of Binuclear [CrLn] (Ln = Gd or Dy) and Trinuclear $[Cr_2Ln]$ (Ln = Gd, Dy, or Tb) Heterometallic Clusters with 2,2′-Bipyridine as Ligand. *Eur. J. Inorg. Chem.* **2015**, *2015* (34), 5702−5707.
(29) Blacque, O.; Amjad, A.; Caneschi, A.; Sorace, L.; Car, P.-E. Synthesis, structure, magnetic and magnetocaloric properties of a series of $\{Cr^{III}_4Ln^{III}\}$ complexes. *New J. Chem.* **2016**, *40* (4), 3571−3577.
(30) Car, P.-E.; Favre, A.; Caneschi, A.; Sessoli, R. Single molecule magnet behaviour in a rare trinuclear $\{Cr^{III}Dy^{III}_2\}$ methoxo-bridged complex. *Dalton Trans.* **2015**, *44* (36), 15769−15773.
(31) (a) Vignesh, K. R.; Soncini, A.; Langley, S. K.; Wernsdorfer, W.; Murray, K. S.; Rajaraman, G. Ferrotoroidic ground state in a heterometallic $\{Cr^{III}Dy^{III}_6\}$ complex displaying slow magnetic relaxation. *Nat. Commun.* **2017**, *8* (1), 1−12. (b) Langley, S. K.; Wielechowski, D. P.; Vieru, V.; Chilton, N. F.; Moubaraki, B.; Chibotaru, L. F.; Murray, K. S. Modulation of slow magnetic relaxation by tuning magnetic exchange in $\{Cr_2Dy_2\}$ single molecule magnets. *Chem. Sci.* **2014**, *5*, 3246. (c) Peng, Y.; Singh, M. K.; Mereacre, V.; Anson, C. E.; Rajaraman, G.; Powell, A. K. Mechanism of magnetisation relaxation in {MIII2DyIII2} (M = Cr, Mn, Fe, Al) "Butterfly" complexes: how important are the transition metal ions here? *Chem. Sci.* **2019**, *10*, 5528.
(32) Langley, S. K.; Le, C.; Ungur, L.; Moubaraki, B.; Abrahams, B. F.; Chibotaru, L. F.; Murray, K. S. Heterometallic 3d-4f single-



https://doi.org/10.1021/acs.cgd.2c00888
*Cryst. Growth Des.* 2023, 23, 197−206

molecule magnets: ligand and metal ion influences on the magnetic relaxation. *Inorg. Chem.* **2015**, *54* (7), 3631−3642.
(33) Langley, S. K.; Forsyth, C. M.; Moubaraki, B.; Murray, K. S. A fluoride bridged $\{Cr^{III}_4Dy^{III}_4\}$ single molecule magnet. *Dalton Trans.* **2015**, *44* (3), 912−915.
(34) Qin, L.; Singleton, J.; Chen, W. P.; Nojiri, H.; Engelhardt, L.; Winpenny, R. E.; Zheng, Y. Z. Quantum Monte Carlo Simulations and High-Field Magnetization Studies of Antiferromagnetic Interactions in a Giant Hetero-Spin Ring. *Angew. Chem., Int. Ed.* **2017**, *56* (52), 16571−16574.
(35) Zhao, X. Q.; Xiang, S.; Wang, J.; Bao, D. X.; Li, Y. C. Magnetic Nature of the CrIII-LnIII Interactions in $[Cr^{III}_2Ln^{III}_3]$ Clusters with Slow Magnetic Relaxation. *ChemistryOpen* **2018**, *7* (2), 192−200.
(36) Xiang, H.; Lu, W.-G.; Zhang, W.-X.; Jiang, L. A $\{Cr_2Dy_4\}$ compressed octahedron: the first sulfate-based single-molecule magnet. *Dalton Trans.* **2013**, *42* (4), 867−870.
(37) Li, Z. Y.; Wang, X. Q.; Zhang, J. J.; Liu, S. Q.; Ni, J.; Sun, Y. J. Synthesis, Structures, and Magnetic Properties of Binuclear [CrLn]-(Ln= Gd or Dy) and Trinuclear $[Cr_2Ln]$(Ln= Gd, Dy, or Tb) Heterometallic Clusters with 2, 2′-Bipyridine as Ligand. *Eur. J. Inorg. Chem.* **2015**, *2015* (34), 5702−5707.
(38) Noodleman, L. Valence bond description of antiferromagnetic coupling in transition metal dimers. *J. Chem. Phys.* **1981**, *74* (10), 5737−5743.
(39) Cundari, T. R.; Stevens, W. J. Effective core potential methods for the lanthanides. *J. Chem. Phys.* **1993**, *98* (7), 5555−5565.
(40) Schäfer, A.; Horn, H.; Ahlrichs, R. Fully optimized contracted Gaussian basis sets for atoms Li to Kr. *J. Chem. Phys.* **1992**, *97* (4), 2571−2577.
(41) Aquilante, F.; Autschbach, J.; Carlson, R. K.; Chibotaru, L. F.; Delcey, M. G.; De Vico, L.; Fdez. Galván, I.; Ferré, N.; Frutos, L. M.; Gagliardi, L.*Molcas 8: New capabilities for multiconfigurational quantum chemical calculations across the periodic table*; Wiley Online Library: 2016.
(42) Heß, B. A.; Marian, C. M.; Wahlgren, U.; Gropen, O. A mean-field spin-orbit method applicable to correlated wavefunctions. *Chem. Phys. Lett.* **1996**, *251* (5−6), 365−371.
(43) Roos, B. O.; Malmqvist, P.-Å. Relativistic quantum chemistry: the multiconfigurational approach. *Phys. Chem. Chem. Phys.* **2004**, *6* (11), 2919−2927.
(44) Roos, B. r. O.; Lindh, R.; Malmqvist, P.-Å.; Veryazov, V.; Widmark, P.-O.; Borin, A. C. New relativistic atomic natural orbital basis sets for lanthanide atoms with applications to the Ce diatom and LuF3. *J. Phys. Chem. A* **2008**, *112* (45), 11431−11435.
(45) Chibotaru, L.; Ungur, L.*The computer programs SINGLE_-ANISO and POLY_ANISO*; University of Leuven, 2006.
(46) Lines, M. Orbital angular momentum in the theory of paramagnetic clusters. *J. Chem. Phys.* **1971**, *55* (6), 2977−2984.
(47) Vieru, V.; Iwahara, N.; Ungur, L.; Chibotaru, L. F. Giant exchange interaction in mixed lanthanides. *Sci. Rep.* **2016**, *6* (1), 1−8.
(48) Fraser, H. W.; Smythe, L.; Dey, S.; Nichol, G. S.; Piligkos, S.; Rajaraman, G.; Brechin, E. K. A simple methodology for constructing ferromagnetically coupled Cr (III) compounds. *Dalton Trans.* **2018**, *47* (24), 8100−8109.
(49) Kollmar, C.; Kahn, O. Is the McConnell mechanism a suitable strategy for the design of molecular ferromagnets? *J. Am. Chem. Soc.* **1991**, *113* (21), 7987−7994.
(50) Rajeshkumar, T.; Singh, S. K.; Rajaraman, G. A computational perspective on magnetic coupling, magneto-structural correlations and magneto-caloric effect of a ferromagnetically coupled {GdIII-GdIII} Pair. *Polyhedron* **2013**, *52*, 1299−1305.
(51) Singh, M. K.; Rajeshkumar, T.; Kumar, R.; Singh, S. K.; Rajaraman, G. Role of (1, 3){Cu-Cu} Interaction on the Magneto-Caloric Effect of Trinuclear {CuII-GdIII-CuII} Complexes: Combined DFT and Experimental Studies. *Inorg. Chem.* **2018**, *57* (4), 1846−1858.
(52) Champion, G.; Lalioti, N.; Tangoulis, V.; Arrio, M.-A.; Sainctavit, P.; Villain, F.; Caneschi, A.; Gatteschi, D.; Giorgetti, C.; Baudelet, F. XMCD for monitoring exchange interactions. The role of the Gd 4f and 5d orbitals in metal-nitronyl nitroxide magnetic chains. *J. Am. Chem. Soc.* **2003**, *125* (27), 8371−8376.
(53) Hallmen, P.; Köppl, C.; Rauhut, G.; Stoll, H.; Van Slageren, J. Fast and reliable ab initio calculation of crystal field splittings in lanthanide complexes. *J. Chem. Phys.* **2017**, *147* (16), 164101.


https://doi.org/10.1021/acs.cgd.2c00888
*Cryst. Growth Des.* 2023, 23, 197−206